AIChE

A Mechanistic Model for Roll Waves for Two-Phase Pipe Flow

George W. Johnson
StatoilHydro ASA, Dept. THE RD MCFA, Research Centre, Porsgrunn NO-3908, Norway

Arnold F. Bertelsen
Dept. of Mathematics, Section of Mechanics, University of Oslo, Blindern NO-0135, Oslo 3, Norway

Jan Nossen
Institute for Energy Technology, Dept. Process and Fluid Flow Tech., Kjeller NO-2027, Norway

DOI 10.1002/aic.11826
Published online September 22, 2009 in Wiley InterScience (www.interscience.wiley.com).

A new two-phase roll wave model is compared with data from high pressure two-phase stratified pipe flow experiments. Results from 754 experiments, including mean wave speed, wave height, pressure gradient, holdup and wave length, are compared with theoretical results. The model was able to predict these physical quantities with good accuracy without introducing any new empirically determined quantities to the two-fluid model equations. This was possible by finding the unique theoretical limit for nonlinear roll amplitude and applying a new approach for determining the friction factor at the gas-liquid interface. © 2009 American Institute of Chemical Engineers
AIChE J, 55: 2788–2795, 2009
Keywords: multiphase flow, fluid mechanics, transport

Introduction

Roll waves have been observed for decades in single and multiphase flows in industrial and environmental applications. Two-phase roll waves are breaking waves which occur at certain flow-rates in stratified gas/liquid duct flow. The waves are sometimes described as bores, periodically distributed along the gas/liquid interface, with less agitated flow between the bores. Hanratty and Hershman[1] described these waves as long wave length disturbances...which might be thought of as surges in the volumetric flow of the liquid. Relatively large amounts of liquid are transported with the waves, particularly under high pressure conditions.

Multiphase flow lines are prevalent in the energy and process industry. For example, a gas condensate transport line operates in the stratified/wavy flow regime, including roll waves under certain conditions. For optimal design and operation of a transport line, it is necessary to correctly predict pressure distribution and liquid level along the line. Commercial multiphase simulators such as OLGA and Tacite provide estimates over a wide range of flow conditions. However, commercial simulators such as these rely heavily on empirical correlations to account for the influence of waves because it is assumed that the gas–liquid interface is flat. Since the wave properties such as amplitude, speed and shape are not determined using OLGA, there exists little physical basis in the models to account for the influence of roll waves on pressure drop and holdup.

Because of high costs and technical hurdles nearly all published stratified flow experiments were performed under atmospheric conditions using air. Detailed measurements of wavy stratified duct flow were performed by Suzanne[2] who mapped the wave-structures in a rectangular duct at atmospheric pressure. Strand[3] mapped the interface structure in wavy stratified pipe flow and measured mean velocity profiles, including secondary flows in the liquid phase. Experiments were performed by Miya[4] in a channel at atmospheric pressure and a correlation for the apparent increase in

Correspondence concerning this article should be addressed to G. W. Johnson at geoj@statoilhydro.com.

interfacial friction due to large waves was suggested. Kowalski[5] and Andritsos[6] suggested empirical correlations for interfacial friction based on experimental data for air-liquid flows in horizontal pipes.

Wu et al.[7] investigated the transition between the roll wave regime and smooth stratified flow at realistic gas condensate conditions in a horizontal 8-inch pipe at 75 bar. Linear stability theory was shown to determine transition to roll waves. Observations of the transition between roll waves and slugging were reported in Kristiansen[8] using Sulfur Hexafluoride and water in a 6.9-cm i.d. horizontal pipe at 8 bar. Holdup and pressure drop were determined in the roll wave regime by Johnson[9] who performed 754 experiments using Sulfur Hexafluoride (SF6) in a 10-cm i.d. pipe at 8 bar. The pipe was inclined at positive angles up to 5° and the transition to roll waves was recorded.

Gravity driven single phase roll waves in an open channel were photographed by Cornish[10] and modeled by Dressler[11] as a first order ordinary differential equation of the form

$$\frac{dh}{dX} = \frac{T(h)}{N(h)} \tag{1}$$

where $h = h(X)$ is the local liquid depth and X is the streamwise position referred to a coordinate system moving with wave speed. Previous work by Thomas[12] on an equation of the same form illustrated that analytical integration was not possible. Using numerical integration, Dressler joined waves using a hydraulic shock condition. At a certain critical liquid depth, Dressler found that the wave speed is equal to the shallow water wave speed for single phase roll waves.

Watson[13] extended Dressler's work to two-phase flows in pipes. However, the solutions were neither unique nor accounted for the relative increase in interfacial friction caused by large waves as seen in a number of experimental investigations. Needham and Merkin[14] and Merkin and Needham[15,16] found solutions to single phase continuous roll wave solutions in open channel flow.

The interfacial friction factor is a key parameter in stratified flow modeling. Andritsos[4] and others have illustrated that modeling the interfacial friction factor equal to the gas-wall friction factor leads to inaccurate predictions for holdup and pressure drop for wavy flows at atmospheric conditions. A summary of existing empirical correlations which used for the interfacial friction in pipe flows can be found in Espedal.[17]

Theory

The cross-sectional averaged fluid velocities are given by

$$U_{\mathrm{k}} = A_{\mathrm{k}}^{-1} \int_{A_{\mathrm{k}}} u_{\mathrm{k}} dA, \tag{2}$$

where u_{k} is the local x-component of the velocity of phase k and A_{k} represents the cross sectional area occupied by the gas and liquid i.e., k = g, l. Long shallow water waves are considered her so that the pressure variations p_{k} in the gas and liquid are given by

$$p_{\mathrm{k}} = P_{\mathrm{ik}} + \rho_{\mathrm{k}} g \cos(h(x) - y) \tag{3}$$

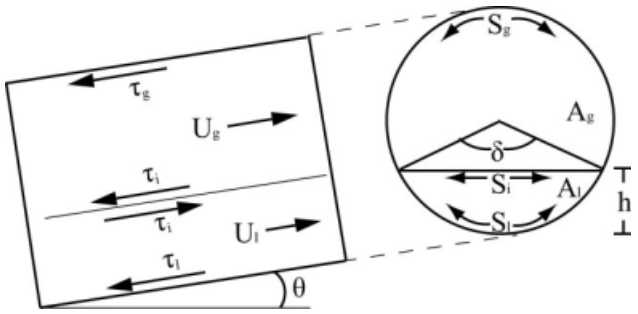

Figure 1. Illustration of the geometrical variables in Eqs. 8–11.

where P_{ik} is the pressure variation at the interface. An illustration of the geometrical quantities such as A_{k}, and the wetted perimeters S_{k} is given in Figure 1. The following cross-sectional averaged one-dimensional mass and momentum balance equations for a two-fluid system were used as the basic equations for our modeling of roll waves in stratified gas/liquid pipe flow

$$\frac{\partial}{\partial t}(\rho_{\mathrm{k}} A_{\mathrm{k}}) + \frac{\partial}{\partial x}(\rho_{\mathrm{k}} A_{\mathrm{k}} U_{\mathrm{k}}) = 0 \tag{4}$$

$$\frac{\partial}{\partial t}(\rho_{\mathrm{l}} A_{\mathrm{l}} U_{\mathrm{l}}) + \frac{\partial}{\partial x}(\Gamma_{\mathrm{l}} \rho_{\mathrm{l}} A_{\mathrm{l}} U_{\mathrm{l}}^2) = -A_{\mathrm{l}} \left(\frac{\partial P_{il}}{\partial x}\right) - \rho_{\mathrm{l}} A_{\mathrm{l}} g \cos\theta \frac{\partial h}{\partial x} - \rho_{\mathrm{l}} A_{\mathrm{l}} g \sin\theta - \tau_{\mathrm{l}} S_{\mathrm{l}} + \tau_{li} S_{\mathrm{i}} \tag{5}$$

$$\frac{\partial}{\partial t}(\rho_{\mathrm{g}} A_{\mathrm{g}} U_{\mathrm{g}}) + \frac{\partial}{\partial x}(\Gamma_{\mathrm{g}} \rho_{\mathrm{g}} A_{\mathrm{g}} U_{\mathrm{g}}^2) = -A_{\mathrm{g}} \left(\frac{\partial P_{\mathrm{ig}}}{\partial x}\right) - \rho_{\mathrm{g}} A_{\mathrm{g}} g \cos\theta \frac{\partial h}{\partial x} - \rho_{\mathrm{g}} A_{\mathrm{g}} g \sin\theta - \tau_{\mathrm{g}} S_g - \tau_{\mathrm{gi}} S_{\mathrm{i}} \tag{6}$$

where τ_{g} and τ_{i} represents the gas and liquid wall shear stress, respectively and $\tau_{\mathrm{k}i}$ represents the shear stresses at the interface for k = g, l. The shape factor Γ_{k} in Eqs. 5 and 6 is defined as

$$\Gamma_{\mathrm{k}} = (A_{\mathrm{k}} U_{\mathrm{k}}^2)^{-1} \int_{A_{\mathrm{k}}} u_{\mathrm{k}}^2 dA \quad \text{for k} = \mathrm{g,l} \tag{7}$$

Mathematical expressions for the geometrical quantities are given below.

$$\delta = 2 \arccos\left(1 - \frac{2h(X)}{D}\right) \tag{8}$$

$$A = \frac{\pi D^2}{4}, \quad A_{\mathrm{l}} = \frac{A}{2\pi}(\delta - \sin\delta), \quad A_{\mathrm{g}} = A - A_{\mathrm{l}} \tag{9}$$

$$S_{\mathrm{g}} = D\left(\pi - \frac{\delta}{2}\right), \quad S_{\mathrm{i}} = D \sin\left(\frac{\delta}{2}\right), \quad S_{\mathrm{l}} = \frac{D\delta}{2} \tag{10}$$

$$D_{\mathrm{l}} = \frac{4A_{\mathrm{l}}}{S_{\mathrm{l}}}, \quad D_{\mathrm{g}} = \frac{4A_{\mathrm{g}}}{(S_i + S_{\mathrm{g}})} \tag{11}$$

where D is the pipe diameter and $h(X)$ the liquid depth (see Figure 1). The stress conditions on the interface are

$$P_{li} - P_{gi} = 2\sigma\kappa, \quad \tau_{li} = \tau_{gi} \tag{12}$$

where σ is the surface tension coefficient and κ is the mean surface curvature. Subject to small mean surface curvature κ and assuming uniform velocity profiles, the following approximations are introduced

$$P_{gi} = P_{li}, \quad \Gamma_g = \Gamma_l = 1 \tag{13}$$

It was assumed that roll waves progress with a constant wave speed C and a relative coordinate system was introduced. Assuming constant fluid densities Eq. 4 becomes

$$\frac{\partial}{\partial X}(-CA_k + A_k U_k) = 0 \tag{14}$$

in the new frame of reference. Equation 14 can be integrated to give

$$U_k = C + \frac{K_k}{A_k} \tag{15}$$

where K_k is the progressive discharge rate for phase k which is constant along the profile of the wave.

Subtracting Eq. 5 from Eq. 6 and applying mass conservation and the approximations given above, we get the profile equation

$$\frac{dh}{dX} = \frac{T}{N} \tag{16}$$

where

$$N = \Delta\rho g H \cos\,\theta - \rho_l (U_l - C)^2 - \rho_g \left(\frac{A_l}{A_g}\right)(U_g - C)^2 \tag{17}$$

and

$$T = H\left[-\Delta\rho g \sin\,\theta + \left(\frac{1}{A_l} + \frac{1}{A_g}\right)\tau_i S_i + \frac{1}{A_g}\tau_g S_g - \frac{1}{A_l}\tau_l S_l\right] \tag{18}$$

with $\Delta\rho = \rho_l - \rho_g$ and $H = A_l/S_i$

Taking the sum of Eqs. 5 and 6 results in an expression for pressure gradient at the interface

$$-\frac{\partial P_i}{\partial X} = \frac{1}{A}\Big(-\rho_g S_i (U_g - C)^2 + \rho_l S_i (U_l - C)^2 + \tau_l S_l + \tau_g S_g + (\rho_g A_g + \rho_l A_l) g \sin\,\theta + \frac{\partial h}{\partial X}(\rho_g A_g + \rho_l A_l) g \cos\,\theta\Big) \tag{19}$$

Eqs. 4–6 are often simplified by assuming fully-developed flow and steady state conditions. In that case Eqs. 4–6 are reduced to

$$\frac{\partial}{\partial x}(A_k U_k) = 0 \tag{20}$$

$$0 = -A_l \frac{\partial P_i}{\partial x} - \rho_l A_l g \sin\,\theta - \tau_l S_l + \tau_i S_i \tag{21}$$

$$0 = -A_g \frac{\partial P_i}{\partial x} - \rho_g A_g g \sin\,\theta - \tau_g S_g - \tau_i S_i \tag{22}$$

The pressure gradient term in Eqs. 21 and 22 can be eliminated using algebraic manipulation to obtain

$$-\Delta\rho g \sin\,\theta + \left(\frac{1}{A_l} + \frac{1}{A_g}\right)\tau_i S_i + \frac{1}{A_g}\tau_g S_g - \frac{1}{A_l}\tau_l S_l = 0 \tag{23}$$

which is equivalent to Eq. 18 at equilibrium i.e., where $T = 0$ The pressure gradient can be found by adding Eqs. 21 and 22 to give

$$-\frac{\partial P_i}{\partial X} = \frac{1}{A}(\tau_l S_l + \tau_g S_g + (\rho_g A_g + \rho_l A_l) g \sin\,\theta) \tag{24}$$

The shear stresses in the basic momentum equations (Eqs. 5–6 and Eqs. 21–22) must be modeled and are given by

$$\tau_k = \frac{1}{8}\rho_k f_k U_k |U_k| \quad \text{for k} = g, l, i \tag{25}$$

where $U_i|U_i| = (U_g - U_l)|(U_g - U_l)|$ and

$$f_k = f_k(Re_k, \varepsilon), \quad f_i = \phi_x f_g(Re_g, \varepsilon) \tag{26}$$

are friction factors where ε is the roughness coefficient of the pipe wall. The factor ϕ_x represents the relationship between the interfacial friction and gas wall friction. The Reynolds numbers are given by

$$Re_k = \frac{U_k D_k}{\upsilon_k} \quad \text{for k} = g, l \tag{27}$$

where υ_k represent the kinematic viscosities. The friction factors must be modeled in Eq. 29 and the following model of Haaland[18] was chosen

$$\frac{1}{\sqrt{f_k}} = -1.8 \cdot \log_{10}\left[\left(\frac{6.9}{Re_k}\right) + \left(\frac{\varepsilon}{3.7D}\right)^{1.11}\right] \tag{28}$$

A value for ϕ_x can be obtained by setting Eqs. 25 and 26 in Eq. 23 and solving for ϕ_x i.e.,

$$\phi_x = 8\left(\frac{\Delta\rho g \sin\theta A_g A_l + \frac{1}{8}\rho_l f_l U_l^2 S_l A_g - \frac{1}{8}\rho_g f_g U_g^2 S_g A_l}{f_g \rho_g (U_g - U_l)|(U_g - U_l)| S_i A}\right) \tag{29}$$

which gives the relative increase in interfacial friction for equilibrium steady state conditions. For identical mean liquid level, the roll wave model and Eq. 29 give identical results for ϕ_x. The method of finding theoretical values for ϕ_x will be explained in the following section.

Roll wave Solutions

Roll wave solutions are found by solving Eq. 16 for given fluid properties, geometry of the pipe and appropriate flow-

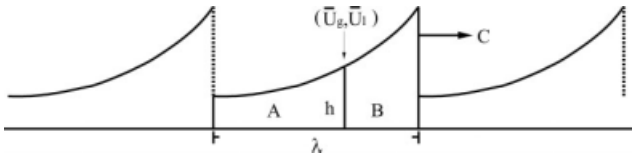

Figure 2. Sketch illustrating the super-critical (A) and sub-critical (B) regions of the theoretical solutions.

The critical liquid depth separates these regions.

rates Q_g and Q_l. Substituting the definitions of A_l, A_g, S_l, S_g and S_i (see Eqs. 8–11) into the definitions of N Eq. 17 and T Eq. 18); Eq. 16 can formally be written as

$$\frac{dh}{dX} = \frac{T(h, U_l, U_g; \phi_x)}{N(h, U_l, U_g; C)} \tag{30}$$

for two-phase flow. The velocities U_k, (k = l, g), appearing in Eq. 30 are functions of $h(X)$, K_k, and C (see Eq. 15), i.e., $U_k = U_k\ (h;\ K_k;\ C)$. Thereby Eq. 30 has the following four unknowns: K_l, K_g, C, and ϕ_x.

The values for K_k (k = l, g) will be defined at the critical liquid level $h = h_0$ by rewriting Eq. 15 as $K_k \equiv (U_{k0} - C)\, A_{k0}$ for k = g, l where

$$U_{l0} \equiv \frac{Q_l}{A_l(h_0)}, \quad U_{g0} \equiv \frac{Q_g}{A_g(h_0)} \tag{31}$$

thereby reducing the number of unknown parameters to a total of three: C, ϕ_x, and h_0. The critical liquid level is defined the unique value for $h = h_0$ which separates the sub-critical and super-critical regions as seen in Figure 2. This specific liquid depth coincides with $T = N = 0$. An assumption was made that the critical liquid height was identical to the mean liquid level $h_0 \equiv \bar{h}$ and therefore, $\bar{h}$ is used to indicate the critical liquid level h_0 throughout the remainder of the text.

One of the main premises of this model was that the theoretically determined value for ϕ_x was a unique value which coincides with the maximum possible roll wave amplitude for a given set of flow-rates. The wave height h_w was defined as

$$h_w = h_d - h_m = h_w(\phi_x; K_l; K_g; \cdots) \tag{32}$$

where h_d is liquid film height at the crest and h_m is the liquid film height at the trough. Together there are five interdependent unknowns: C, ϕ_x, h_m, h_0, and h_d which were determined simultaneously using a Newton-Raphson solver for nonlinear equations.

Five conditions are needed to determine C, ϕ_x, h_m, $\bar{h}$, and h_d viz.

1) $N = 0$ at $h = \bar{h}$
2) $T = 0$ at $h = \bar{h}$
3) $T = 0$ at $h = h_m$
4) $N = 0$ at $h = h_d$
5) $[S] = 0$ at $h = h_m, h_d$

where the hydraulic jump condition represented by condition 5) was given by

$$[S] = \left[\Delta\rho g h \cos\theta + \frac{1}{2}\rho_l (U_l - C)^2 - \frac{1}{2}\rho_g (U_g - C)^2\right] = 0 \tag{33}$$

which was applied at h_m and h_d. The solver required initial values for C, ϕ_x, h_m, $\bar{h}$, and h_d and a solution was not always forthcoming due to the nature of nonlinear root solvers.

Conditions (1) and (2) represent the requirement that Eq. 30 is regular at the critical liquid level. Conditions (3) and (4) can be justified by requiring that the function $h(X)$ is a monotone increasing function of X i.e., the liquid liquid level consistently increases from the trough to the crest. Therefore, $dh/dX > 0$ which necessitates that either $T > 0$ and $N > 0$ or $T < 0$ and $N < 0$ for all $h(X)$. This is equivalent to ensuring that the product

$$TN \geq 0 \tag{34}$$

The values h_m and h_d are precisely the values for h where the product TN changes sign (see Figure 3). Hence, conditions (3) and (4) provide a simple way of determining the maximum possible wave height.

Given that the Newton-Raphson solver determined the roots (i.e., C, ϕ_x, h_m, $\bar{h}$, and h_d) of the five nonlinear equations listed earlier. The following restrictions were applied to ensure unique physical solutions.

1) $h_d > \bar{h} > h_m$
2) $dU_k/dh > 0$ for $h \in [h_m, h_d]$
3) $C > U_l$ for $h \in [h_m, h_d]$
4) $dN/dh > 0$ and $dT/dh > 0$ at $h = \bar{h}$

Requirement (1) is self-evident but was needed in our case to prevent the solver from assigning correct values to the incorrect parameter names. The second and third requirements ensure that the fluid velocities increase with increasing liquid depth, in the relative coordinate system, and the wave speed is always greater than the liquid velocity respectively.

Requirement (4) was necessary to ensure that the solution $h(X)$ to Eq. 30 is a monotonic increasing function of X. See

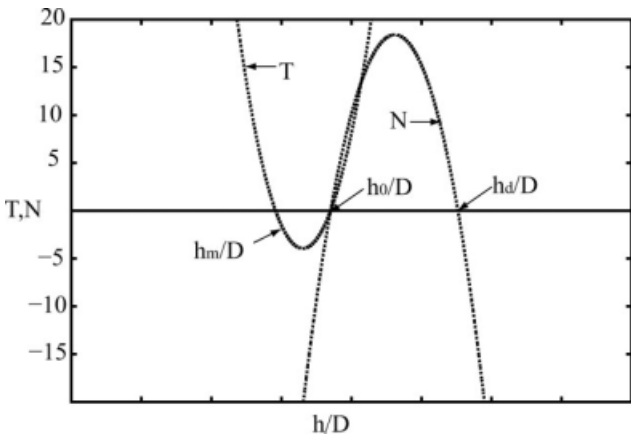

Figure 3. Figure showing the required qualitative behavior of Eqs. 17 and 18, where Eq. 18 was multiplied by 100 to make the functions the same order of magnitude for the illustration.

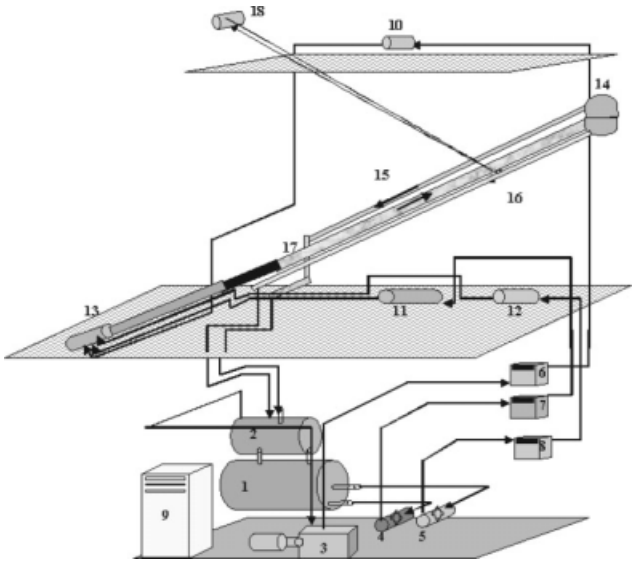

Figure 4. Experimental facility capable of three phase flows.

Located on three floors where G. (Gas), W. (Water), O (Oil). 1, O.-W. separator; 2, G.-W. separator; 3, G. compressor; 4, W. pumps; 5, O. pump; 6, G. heat exchanger; 7, W. heat exchanger; 8, O. heat exchanger; 9, Main switch board; 10, G. turbine meter; 11, W. elec. magn. Meter; 12, O. coriolis meter; 13, inlet mixing section; 14, Preseparator; 15, G. return pipe; 16, liquid return pipe; 17, Pipe; 18, Winch.

Figure 3 for an illustration of the qualitative behavior of T and N for a valid roll wave solution which fulfills the aforementioned requirements. With C, ϕ_x, h_m, $\overline{h}$, and h_d determined, Eq. 30 can be solved for $h(X)$ and the shape of the wave found.

By solving the set of five nonlinear equations, a unique solution for C, ϕ_x, h_m, $\overline{h}$, and h_d was obtained. The determination of wave length was found by using the following definition

$$\lambda = \int_{X_m}^{X_d} dX = X_d - X_m \tag{35}$$

but this is not very useful here, since X_d and X_m are not readily determined. A change of variables by reformulating Eq. 30, $dX = (NT^{-1})dh$, gives

$$\lambda = \int_{h_m}^{h_d} \left(\frac{N}{T}\right) dh \tag{36}$$

To ensure consistency with the model assumption $\overline{h} = h_0$ and to obtain finite wave lengths, a new parameter $\widehat{h}_m$ is introduced in Eq. 36 so that

$$\widehat{\lambda} = -\int_{h_d}^{\widehat{h}_m} \left(\frac{N}{T}\right) dh \tag{37}$$

Two unknowns $\widehat{\lambda}$ and $\widehat{h}_m$ exist in Eq. 37 and an additional equation was needed which was provided by the definition of the mean liquid height

$$\overline{h} = -\widehat{\lambda}^{-1} \int_{h_d}^{\widehat{h}_m} h(X) \left(\frac{N}{T}\right) dh \tag{38}$$

Eqs. 37 and 38 can be combined to give

$$\int_{h_d}^{\widehat{h}_m} \left(\frac{N}{T}\right) \left(\frac{h}{\overline{h}} - 1\right) dh = 0 \tag{39}$$

which can be solved for the $\widehat{h}_m$. Thereafter the wave length is determined using Eq. 37 and the wave height is now given by

$$\widehat{h}_w = h_d - \widehat{h}_m \tag{40}$$

Hence, a unique wave length, wave height, wave speed, mean liquid level and the ratio $\phi_x = f_i/f_g$ were determined without introducing new empirically determined quantities to the two-fluid equations.

Finally, the average pressure drop per unit wave length for the system was equal to the pressure drop averaged over a single wave because all waves are identical. The pressure gradient averaged is obtained using

$$\frac{\overline{\partial P_i}}{\partial X} = \widehat{\lambda}^{-1} \int_{\widehat{h}_m}^{h_d} \frac{\partial P_i}{\partial X} \left(\frac{N}{T}\right) dh \tag{41}$$

The pressure drop over the shock was assumed to be negligible compared to the pressure drop over the entire wave of length $\widehat{\lambda}$.

Experimental Setup and Analysis

The experiments were performed at The Institute for Energy Technology (IFE) in Kjeller, Norway. Figure 4 illustrates the experimental facility. Sulfur Hexafluoride (SF6), with a density of $\rho_g = 50$ kg/m^3 and dynamic viscosity of $\mu_g = 1.61 \cdot 10^{-5}$ kg/ms, was chosen for the gas phase. Water was chosen for the liquid phase with a density was $\rho_l = 998$ kg/m^3 and dynamic viscosity of $\mu_l = 9.98 \cdot 10^{-4}$ kg/ms. The gas and liquid temperature was held constant at $\approx$20°C using separate counter current heat exchangers. The general specifications of the laboratory components used in the experiments are given in Table 1.

Experiments were performed at $\theta = 0.00°$, 0.10°, 0.25°, 1.00°, 2.50°, and 5.00° in a 25-m-long 10-cm i.d. pipe. The number of experiments at each angle was 150, 172, 161, 114, 90, and 67 respectively. The pipe was inclined using an electrical winch. An inclinometer determined the pipe inclination with an accuracy of 0.1°

Table 1. Dimensions and Ranges of the Pipe and Pumps

Maximum pressure	10 bar
Test section length	25 m
Test section diameter	10 cm i.d.
Superficial gas velocity	0.3–12 m/s
Superficial liquid velocity	0.0005-2.0 m/s
Inclination	0–90°

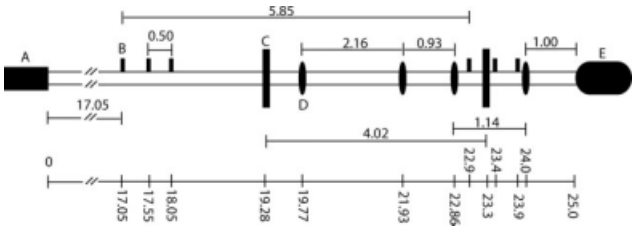

Figure 5. Indication of the relative placements of the inlet (A), pressure sample points (B), gamma densitometers (C), wave probes (D) and outlet (E).

The experimental pressure drop $-dP^e/dX$ and mean liquid height h^e were obtained using three differential pressure transducers, four specially designed conductivity parallel-wire wave probes and two broad-beam γ-densitometers. The wave probes consisted of 400-μm diameter platinum wires separated by 3 mm. Liquid level was linearly dependent on the measured conductivity between the wires. The differential pressure transducers were sampled at $\approx$3 Hz while the wave probes and densitometers were sampled at 50 Hz. Time averaged values for pressure drop and liquid level were obtained by averaging over 81.92 s.

The pressure transducers had an operating range of 2000 Pa and an accuracy of 0.10% FSO which gave a maximum error of 2 Pa. The gamma densitometers were accurate to within $\pm$0.02 (absolute).

All instrumentation was located within the final $\approx$8-m section of the 25-m long pipe which is shown in Figure 5. Therefore, the flow had $\approx$17 m or 170 equivalent pipe diameters to develop. The wave probe and pressure tap closest to the outlet were located was 1 m from the outlet. The flow was fully developed at the gas and liquid rates which allowed the formation of roll waves.

The pipe wall roughness coefficient was determined using single phase gas pressure drop measurements at a number of U_{sg} values. The final value was determined to be $\varepsilon = 2{\cdot}10^{-5}$ m.

Cross-correlations and power spectra were calculated for each experiment to obtain the experimental wave speed C^e and dominating wave frequency f^e, respectively. Wave length was determined using $\lambda^e = C^e / f^e$ Roll waves generally had frequencies $f^e < 1$ Hz which only allowed first order estimates for wave length to be made.

Mean wave heights were found using the following expression

$$h_\sigma = 2\sqrt{2}\sigma_s \tag{42}$$

where σ_s is the RMS standard deviation of the liquid height time trace $h^e(t)$

Comparison Between Measurements and Predictions

Four types of waves were observed in the experimental study: capillary waves, 2D waves, 3D waves and roll waves. Capillary waves had very small amplitudes and short wavelengths. 2D waves were smooth gravity waves where the front and back sides of the waves were roughly symmetric. As opposed to 2D waves, 3D waves varied across the pipe cross section and gave the appearance of a chaotic interface. Roll waves had breaking fronts, long wavelengths and were easily identifiable.

Roll waves were observed to be initiated due to two mechanisms which are listed below

1) Large 2D waves of differing velocities merged forming roll waves at large liquid rates and low gas rates in the presence of 3D waves.

2) For large gas rates and low liquid rates a very long undulation (swinging) of the interface eventually developed into roll waves.

A regime was classified as "roll wave" when periodic roll waves were observable both visually and through time trace data. The classification of slug flow was made when a discernible persistent liquid slug was visually observed. See Kristiansen[8] for an experimental investigation under high system pressure which specifically focuses on the transition between roll waves and slug flow.

Theoretical roll wave solutions were obtained for most of the experimental data points. The numerical algorithm produced a solution within 1 s in most cases. A comparison was made between the roll wave model predictions and corresponding observations for mean liquid level, pressure drop and wave properties. The relative increase in interfacial friction $\phi_x = f_i/f_g$ was determined experimentally using Eq. 29 and compared with corresponding theoretical values.

The accuracy of the values for ϕ_x using Eq. 29 depended on the accuracy of the friction model (Eq. 28) and the accuracy of the measured liquid level. An indication of how well the gas and liquid friction factors performed was made by comparing Eq. 24 with measured pressure drops for each experiment. Using the measured mean liquid level, Eq. 24 gave pressure drop values which were less than measured values by $\approx$20.9% on average for horizontal flow. The theoretical and measured pressure drop compared slightly better for upward inclinations. This indicated that the sum of the actual gas and liquid shear stresses were larger than the theoretical shear stresses which were modeled using Eqs. 25–28. Espedal[17] found larger under-predictions for air-water flows using the Haaland friction model than was found here.

Theoretical values for ϕ_x differed from measured values using Eq. 29 by 5.6%, 3.7%, 2.7%, 11%, $-$5.6%, and $-$38.6% at $\theta = 0.00^\circ$, 0.10°, 0.25°, 1.00°, 2.50°, and 5.00°, respectively. Although overall agreement was excellent at small inclinations the roll wave model generally gave values which were too low at low liquid flowrates and too high at large liquid flowrates. Larger differences were found at 5.00° due to very low theoretical values for ϕ_x at low liquid rates.

The experimental values for mean liquid level differed from model predictions by $\sim$7% at pipe inclinations up to 2.50° as shown in Table 2 and Figure 6. Larger differences between the model and observations for mean liquid level were observed for angles $2.50^\circ \leq \theta$.

The predicted pressure gradient using Eq. 41 differed from experimental measurements by $\approx$3% for $\theta < 2.50^\circ$ For large gas rates and low liquid rates the model continued to predict the pressure gradient within 10% even at relatively large pipe inclinations as seen in Figure 7. The roll wave model managed to predict pressure drop accurately because the shear stresses varied along the wave. Pressure drop was

Table 2. Average Percentage Difference Between Theoretical Solutions and Measurements

θ	N	h/D	C	$-(dP_i/dx)$	h_σ
0.00	150	6	−17	0	3
0.10	172	5	−17	2	−2
0.25	161	7	−17	1	−8
1.00	114	5	−22	3	−43
2.50	65	11	−41	11	−71
5.00	25	11	−43	23	−81

The symbol n represents the number of theoretical solutions which were found.

a large at the wave crests due to the large fluid velocities which gave relatively large theoretical values for the shear stresses. Therefore the crest of the waves contributed to a larger average pressure drop using Eqs. 19 and 41 than was obtained at the same mean liquid level using Eq. 24.

Qualitative agreement was found between the theoretical values for ϕ_x which were obtained from the roll wave model and the values which were obtained using Eq. 29. Both the experimental and theoretical values for ϕ_x increased with increasing mixture velocities $U_{\text{mix}} = (U_{\text{sg}} + U_{\text{sl}})$ at all angles. However, a simple analysis of Eq. 29 revealed an interesting result. Relatively large changes in ϕ_x accompany small differences in mean liquid level. For example, using the following variables in Eq. 29, ($U_{\text{sg}} = 4.00$, $U_{\text{sl}} = 0.20$, $\theta = 0.00$) at the measured liquid level $h/D = 0.196$, $\phi_x = 4.971$, but choosing a slightly smaller liquid level $h/D = 0.186$, Eq. 29 gave $\phi_x = 6.635$. In this example a 5% difference in liquid level gave a 33% increase in ϕ_x. This indicated that relatively large percentage differences for ϕ_x had relatively little impact on liquid level. This was seen when a number of flowrates combinations and pipe inclinations were investigated in this way. Although small percentage differences were found between theoretical and measured liquid level, a greater percentage difference between theoretical ϕ_x values was obtained with the roll wave model and observed values for ϕ_x using Eq. 29.

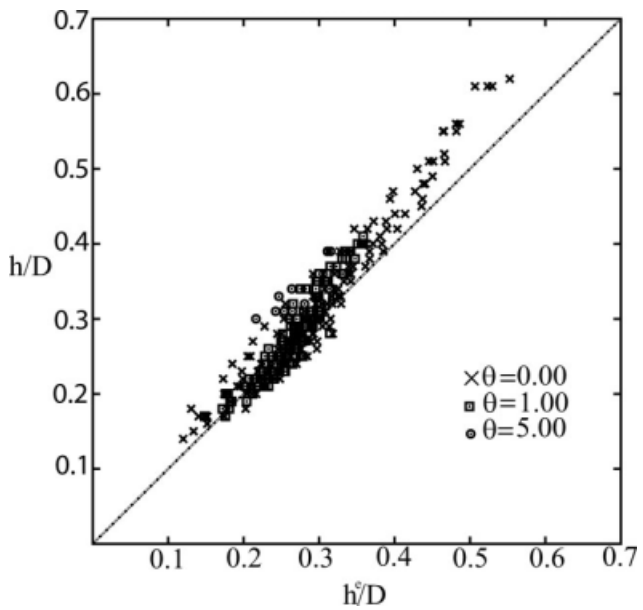

Figure 6. Model predictions for mean liquid height compared with measurements.

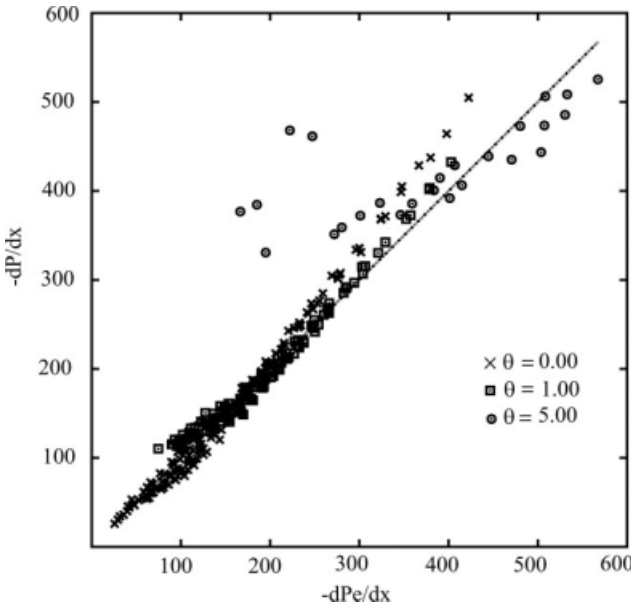

Figure 7. Model predictions for pressure gradient compared with measurements.

The nonlinear wave speeds determined by the model were generally 17% lower than measured wave speeds at $\theta < 2.50°$ Both the measured wave speeds and theoretical waves speeds increased with increasing U_{mix}. Linear stability theory which is frequently used for determining theoretical wave speed, predicts yet lower wave speeds. This model gave reasonable estimates and correct qualitative behavior.

The wave height was determined using Eq. 40 for the theoretical waves and Eq. 42 for the observed waves. Generally the wave model under-predicted wave amplitudes, but similar qualitative agreement existed even though the two approaches are fundamentally different. The experimentally determined wave height was based on statistical analysis of the variations at the interface while wave height using the roll wave model was determined using Eq. 40. A comparison

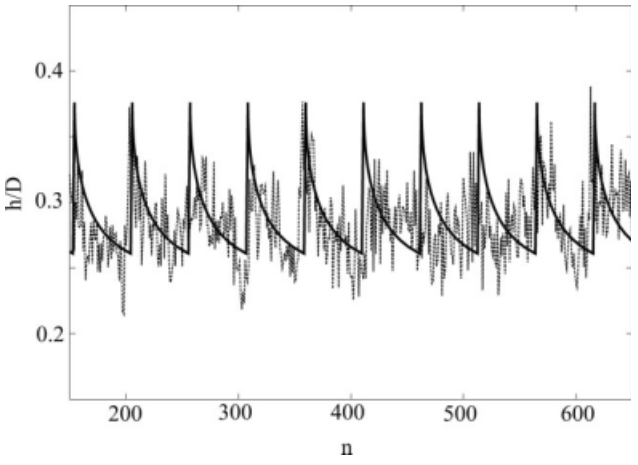

Figure 8. Example of a 12 s time segment from an experimental time trace (dashed line) compared with a theoretical solution.

between a theoretical solution for $h(X)$ and a typical time trace of the liquid height is shown in Figure 8 where complex smaller scale variations at the interface were apparent relative to the idealized theoretical solution.

Concluding Remarks

The roll wave model presented here was able to determine a unique wave which matched mean liquid level and pressure drop well at low inclinations. The predictions using the wave model were more accurate than OLGA which had an error >15%. The detailed properties of roll waves such wave speed, wave height and wave length were predicted less accurately.

It was shown that less accurate solutions for liquid level and pressure drop were obtained at upward inclinations. This could partly be attributed to increasingly nonuniform velocity profiles at larger inclinations and small flow-rates. Furthermore, droplets and bubbles were prevalent in many of the experiments. Predictions for large gas rates and low liquid rates gave good agreement at all angles.

It is generally agreed upon that one of the primary challenges in two-phase modeling is the proper modeling of the interfacial friction. A number of researchers have suggested empirical correlations based on experimental data which work well for given fluid physical properties and pipe dimensions. A completely new approach was taken to obtain the increase in interfacial friction due to large waves which did not rely on experimental data. This approach should have better extrapolation properties than the traditional approach of developing correlations based on specific data sets. Furthermore, the predicted variables such as nonlinear wave speed, wave height and length provide useful information which could be used as a basis for further modeling.

Notation

A, A_k = cross sectional area of the pipe and for the gas and liquid layers (m^2)
C, C^e = wave speed (theoretical and measured) (m s^{-1})
D, D_k = pipe diameter and hydraulic diameters (m)
f_k = friction factors
g = acceleration of gravity (m s^{-2})
H = equivalent diameter A_l/S_i (m)
h, h^e = liquid level (theoretical and measured) (m)
h_0 = critical liquid level (m)
h_m, h_d = theoretical minimum and maximum liquid heights (trough and crest depths, m)
h_σ = wave height (m)
K_k = progressive discharge rates (m^3 s^{-1})
P_i = pressure at the interface (kg m^{-1} s^{-2})
Q_k = flowrates for each phase (m^3 s^{-1})
Re_k = Reynolds number for each phase
S_k = wetted perimeters for (m)
u_k, U_k = axial velocity component, average axial velocity component (mv s^{-1})
U_{sk} = superficial velocity for (m s^{-1})
U_{mix} = sum of the superficial velocities ($h_k + U_{si}$) (m s^{-1})
X = axial coordinate (m)

Greek letters

Γ_k = shape factors
δ = angle from the pipe centerline to the interface
ε = pipe surface roughness coefficient (m)
θ = angle
κ = mean surface curvature (m^{-1})
λ, λ^e = wave length (theoretical and measured) (m)
ν_k = kinematic viscosities for phase k (m^2 s^{-1})
ρ_k = density for phase k (kg m^{-3})
σ = surface tension (kg s^{-2})
σ_s = standard deviation
τ_k = shear stresses (kg m^{-1} s^{-2})
ϕ_x = ratio between f_i/f_g

Subscripts/superscripts

e = experimental value
g = gas
i = interface
k = indicator for the gas (g), liquid (l) and interface (i)
l = liquid

Literature Cited

1. Hanratty TJ, Hershman A. Initiation of roll waves. *AIChE J*. 1961;7:488–497.
2. Suzanne C. Stucture de l'ecoulement stratifie de gaz et de liquide en canal rectangulaire. Ph.D. Thesis, Institut National Polytechnique de Toulouse, France 1985.
3. Strand Ø. An experimental investigation of stratified two-phase flow in horizontal pipes, Ph.D. Thesis, University of Oslo, Oslo, Norway 1993.
4. Miya M, Woodsmansee DE, Hanratty TJ. A model for roll waves in gas-liquid flow. *Chem Eng Sci*. 1971;26:1915–1931.
5. Kowalski JE. Interfacial shear stress in stratified flow in a horizontal pipe. *AIChE J*. 1987;33:274–281.
6. Andritsos N. Effect of pipe diameter and liquid viscosity on horizontal stratified flow. Ph.D. Thesis, University of Illinois, Urbana-Champaign, 1986.
7. Wu HL, Pots BFM, Hollenberg JF, Meerhoff R. Flow pattern transitions in two-phase gas/condensate flow at high pressure in an 8-inch horizontal pipe. *Third Int Conf Multi-Phase Flow*. 1987;A2:13–21.
8. Kristiansen O. Experiments on the transition from stratified to slug flow in multiphase pipe flow. Ph.D. Thesis, Norwegian University of Science and Technology, Trondheim, 2004.
9. Johnson GW. A study of stratified gas liquid flow. Ph.D. Thesis, University of Oslo, Oslo, Norway 2005.
10. Cornish V. *Ocean Waves and Kindred Geophysical Phenomena*. London: Cambridge University Press, 1934.
11. Dressler RF. Mathematical solution of the problem of roll-waves in inclined open channels. *Commun Pure Appl Math*. 1949;2:149–194.
12. Thomas H. The propagation of stable wave configurations in steep channels. In: *Technical Report*. Pittsburgh, PA: Carnegie Institute of Technology, 1937.
13. Watson, M. Wavy stratified flow and the transition to slug flow. In: *Multi-Phase Flow Proceedings of the fourth International Conference*, BHRA, Nice, France 1989:495–512.
14. Needham DJ, Merkin JH. A note on the stability and the bifurcation to periodic solutions for wave-hierarchy problems with dissipation. *Acta Mech*. 1984;54:75–85.
15. Merkin JH, Needham DJ. An infinite period bifurcation arising in roll waves down an open inclined channel. *Proc R Soc Lond*. 1986;405:103–116.
16. Merkin JH, Needham DJ. On infinite period bifurcations with an application to roll waves. *Acta Mech*. 1986;60:1–16.
17. Espedal M. An Experimental of stratified two-phase pipe flow at small inclinations. Ph.D. Thesis, University of Oslo, Oslo, Norway 1998.
18. Haaland SE. Simple and explicit formulas for the friction factor in turbulent pipe flow. *J Fluids Eng*. 1983;105:89–90.

Manuscript received July 8, 2008, and revision received Dec. 15, 2008.